Regional Environmental Change (2022) 22:132
https://doi.org/10.1007/s10113-022-01978-0

ORIGINAL ARTICLE

Forest expansion in abandoned agricultural lands has limited effect to offset carbon emissions from Central-North Spain

Eduardo Velázquez[1,2] · Carolina Martínez-Jaraíz[3] · Charlotte Wheeler[4] · Edward T. A. Mitchard[4] · Felipe Bravo[1,2]

Received: 1 March 2022 / Accepted: 17 September 2022 / Published online: 15 November 2022

Abstract

We assessed the process of carbon (C) accumulation as a consequence of forest expansion in abandoned agricultural lands over the period 1977–2017 in a vast (9.4 million ha) area of Mediterranean continental environment in Central-North Spain. We achieved this objective, through obtaining AGC and BGC estimations based on direct field measurements taken in 30 plots (25 m × 25 m), and extrapolating to the landscape using *Synthetic Aperture Radar* (SAR) satellite data from 2018. Using aerial photographs and forest maps, we found that 145,193 ha of agricultural land in 1957 (1.54% of the study regions' total area) has since then regenerated naturally to forests and woodlands. Although mean AGC and BGC densities were modest (i.e. 18.04 and 6.78 Mg C ha^{-1}), they reached relatively large maximum values (i.e. 60 and 21 Mg C ha^{-1}). The BGC stock was also very large, representing 37.3% of the total C stock (10 Tg) accumulated. However, we detected a mean annual C sink of 0.25 Tg C·$year^{-1}$ which barely offset 1.22% of the total regional CO_2 emissions. Our findings point to a smaller sequestration potential under Mediterranean continental than under temperate-cold conditions. Nonetheless, the area affected by this process could be larger than detected and many of the recovering lands might have not still reached their C uptake peak. If such lands are to be used to store C, we strongly advocate for the application of active forest management measures to increase their CO_2 sequestration potential.

Keywords Ecological succession · Allometric equations · Above-ground carbon · Below-ground carbon · SAR backscatter · Regression

Communicated by Victor Resco de Dios

✉ Eduardo Velázquez
eduardo.velazquez@forest.uva.es

Carolina Martínez-Jaraíz
camartinezja@gmail.com

Charlotte Wheeler
cwheeler@ed.ac.uk

Edward T. A. Mitchard
edward.mitchard@ed.ac.uk

Felipe Bravo
fbravo@pvs.uva.es

[1] Instituto Universitario de Gestión Forestal Sostenible, Universidad de Valladolid, Avda. de Madrid 44, 34004 Palencia, Spain

[2] Escuela de Ingenierías Agrarias, Universidad de Valladolid, Palencia, Spain

[3] Stipa and Azeral S.L., Cuenca, Spain

[4] School of Geosciences, University of Edinburgh, Edinburgh, UK

Introduction

Land-use and land-cover changes (LULCC) are largely responsible for the net flux of CO_2 between terrestrial ecosystems and the atmosphere, and therefore, they are major driving forces of the terrestrial carbon cycle (Houghton 2010). For instance, over the last decades, in temperate regions, there has been a net uptake of carbon (C) by terrestrial ecosystems which can be partially explained by the positive impact of forest regrowth, afforestation, reforestation, fire suppression, and forest expansion on abandoned agricultural lands in atmospheric CO_2 sequestration (Pan et al. 2011; Sitch et al. 2015). Forest expansion in abandoned agricultural lands, also referred as the *forest transition* (e.g. Barbier et al. 2009), often occurs as a consequence of rural–urban migration processes which lead to the abandonment of areas formerly subjected to agrarian uses, and is usually more pronounced in remote regions or in areas of shallow, poorly drained or stony soils, and/or steep slopes, where agricultural productivity is low and mechanisation is

often restricted (Cramer et al. 2008). As soon as agrarian uses cease, spontaneous revegetation of these abandoned lands or *old-fields* starts, and they are progressively replaced by shrublands, woodlands, and forests.

The biomass C accumulated as a consequence of forest expansion in abandoned agricultural lands has been mainly estimated through simulation models based in historical agricultural and forest inventory statistics (Rhemtulla et al. 2009; Kuemmerle et al. 2011; Schierhorn et al. 2013). During the last decade, methodological approaches combining field and remote sensing data have been also increasingly used as a cost-effective means to map and reliably estimate forest live C stocks over large geographical areas (e.g. McNicol et al. 2018). In particular, we can use active sensors such as *Synthetic Aperture Radar* (SAR), which send out a beam of microwave energy to the land surface, and explore the relationships between above-ground biomass (AGB) and the quantity of backscatter, i.e. the energy that returns to the sensor once it has interacted with the structural elements of the vegetation (i.e. trunks, branches, and foliage) and the soil. The SAR backscatter is able to provide information of the tridimensional structure of the forests, which in turn responds largely to their biomass, with higher backscatter values recorded in areas with higher woody biomass in the vegetation (Woodhouse 2006; Mitchard et al. 2009). As the amount of C stored in the AGB can be easily extracted through conversion factors, we can also easily relate the SAR backscatter to the above-ground carbon (AGC). For long wavelength (> 20 cm) L- and P-band sensors, most of the backscatter comes directly from tree trunks and large branches (Woodhouse 2006). Therefore, these sensors are particularly appropriate for estimating AGB and AGC stocks (Mitchard et al. 2009, 2011). The backscatter also varies with the type of polarisation (i.e. the way in which the microwave energy is transmitted to the land surface and it is received in the sensor). Horizontal-transmit, Vertical-receive (HV) polarisations exhibit generally a greater sensitivity to tree structures than Horizontal-transmit, Horizontal-receive (HH) ones (McNicol et al. 2018), but the opposite occurs in uneven-age, vertically stratified, and diverse forests (Woodhouse 2006), where is highly recommendable to use all available polarisations in order to make accurate estimations of AGC stocks. More information on the different techniques used to map forest biomass and C through methods combining field measurements and SAR data is available in Lu (2006), Woodhouse (2006), and Goetz et al. (2009).

In the last decade, the live C stocks developed as a consequence of forest expansion after agricultural land abandonment has been estimated through large, regional, scales in temperate cold environments of the Eastern and Midwestern USA (e.g. Rhemtulla et al. 2009), and Eastern Europe (e.g. Kuemmerle et al. 2011; Schierhorn et al. 2013). By contrast, in Southern Europe, where this process has been also widespread (Beilin et al. 2014; Lasanta et al. 2021), to our knowledge, most of the estimates of the C accumulated have been performed locally (e.g. Calvão and Palmeirim 2004; Chrysafis et al. 2017), with those at regional scale lacking (Galidaki et al. 2016). Moreover, most of the aforementioned local studies have quantified the above- but not the below-ground carbon. The carbon stored in this compartment should be considered in all live forest C estimations (Saatchi et al. 2011), but especially in ecosystems experiencing an annual dry period such as Mediterranean ones, where plants invest more resources belowground (Canadell et al. 1996). Furthermore, the estimation of Mediterranean forest C pools through approaches combining field and SAR data is particularly challenging due to the high spatial fragmentation (Alivernini et al. 2016), heterogeneity, and structural complexity of these systems, which usually comprise different forest types (Laurin et al. 2018). However, as the countries in the Mediterranean basin will be particularly affected by climate change (Kovats et al. 2014), the assessment of the C stocks accumulated after agricultural land abandonment might be particularly important to update their C budgets and improve the national reporting in the framework of the Paris Agreements. It might also help to identify positive and negative trade-offs amongst competing land-use options (e.g. Kuemmerle et al. 2011) and to develop active forest policies for these naturally reforested areas.

In this study, we aim to provide a reliable estimation of the C stocks developed as a consequence of forest expansion in abandoned agricultural lands, and their spatial distribution, in a large region of Central-North Spain, over the period 1977–2017. To attain this objective, we used a combination of field inventory, ortho-corrected historical images, and SAR data. Specifically, we hypothesised that (i) the area affected by forest expansion in abandoned agricultural lands has occupied a proportion of the total area of the study region similar to those detected in other regions in which this process has been also studied; (ii) the C density, the total C stocks, and the rate of C sequestration of the below-ground biomass pool have been relatively important compared to those of the above-ground biomass one; (iii) the rate of C sequestration of the total C pool has been enough to offset an important proportion of regional CO_2 emissions.

Material and methods

Study area

The study was conducted in *Castilla y Léon*, a 9.4 million–ha region which occupies a high plateau (700–900 m a.s.l.) almost completely surrounded by mountain ranges (> 2500 m a.s.l.; Fig. 1a–b). This area has a Mediterranean continental climate, with warm and dry summers and cold

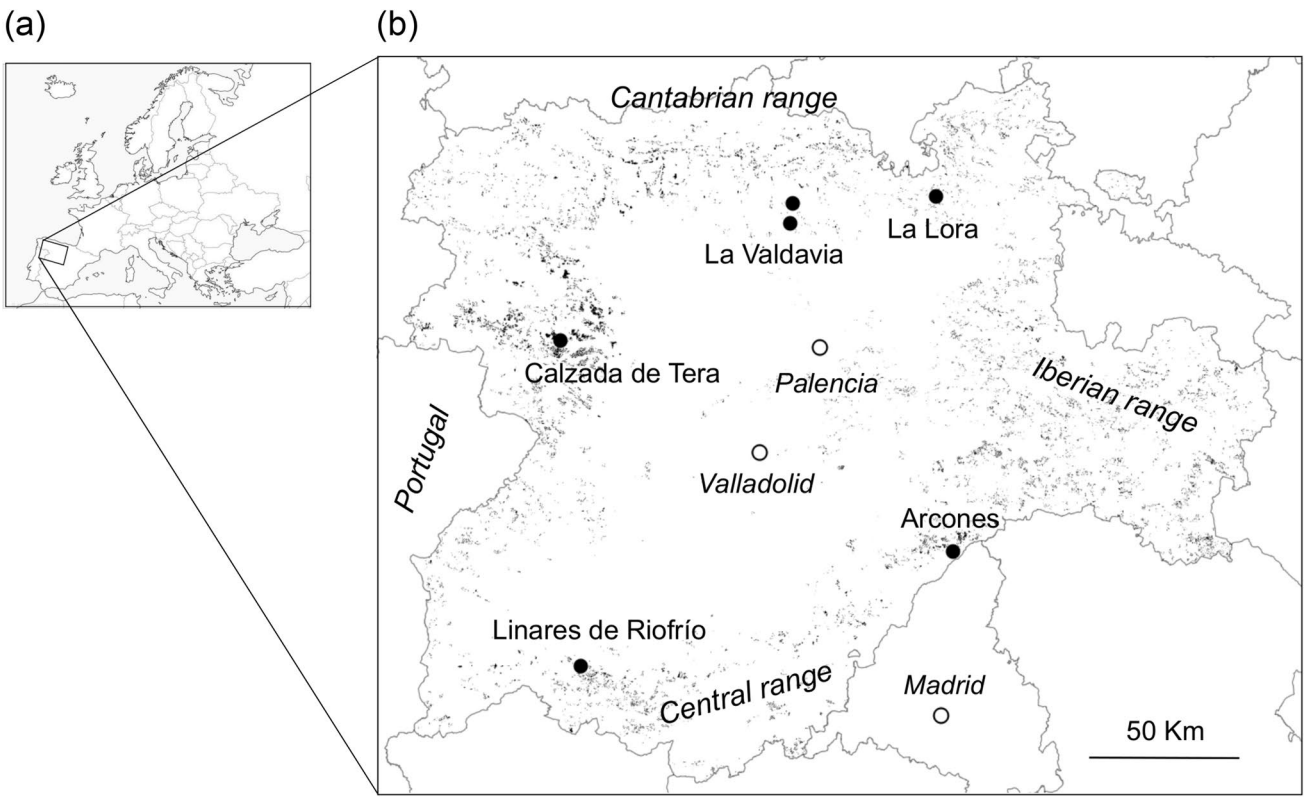

Fig. 1 (**a**) Location of the study area in Europe and (**b**) map of the study area, showing the area occupied by recovering lands over the period 1977–2018 (in grey), as well as the regional limits, as well as the locations of mountain ranges, main cities (white points), and the five study areas (black points)

winters, and shows large variations in mean annual rainfall (i.e. 500–1800 mm/year) as a consequence of its heterogeneous physical environment. In this region, human population increased until the 1950s, and then declined mainly as a consequence of marked rural–urban migration processes, which in turn left large areas of crop, pastures, and fallow lands devoid of their former uses and abandoned (Gil-Sánchez and Torre-Antón 2007).

Mapping agricultural abandonment

To determine the area affected by forest expansion in abandoned agricultural lands, we first split the study area into their four main forests types, i.e. those occupying a major area, according to the 1:50,000 *Spanish Forest Map* (Área Banco de Datos de la Naturaleza, 2006). These four forest types were dominated by a juniper tree (*Juniperus thurifera*), a perennial oak (*Quercus ilex*), and two semi-deciduous oaks (*Q. pyrenaica* and *Q. faginea*). Second, for the areas occupied by these forest types, we obtained aerial photographs for the periods 1977–1980 (i.e. the first to be ortho-corrected and at high resolution, and therefore showing high enough quality for analysis) and 2015–2017 from the Centro Nacional de Información Geográfica. Third, we superposed the aerial photographs of 1977–1980, with the areas occupied by the four main forest types selected. In all the superposed regions, we digitised as agricultural lands those areas showing little or no tree cover and features such as ploughing lines, stone walls, and/or hedgerows, which indicated their former use as crop or pastured lands. Fourth, we checked whether these agricultural lands become vegetated in the aerial photos of the most recent period: 2015–2017. In such cases, we assumed that forest expansion had occurred on that land (Aggenbach et al. 2017). Once we determined the area occupied by forests, woodlands, and other wooded lands developed as a consequence of agricultural land abandonment (hereafter; recovering lands), we located five study sites based on literature references (e.g. Allende-Álvarez et al. 1997) and expert knowledge. Amongst these sites, two of them (La Valdavia and Linares de Riofrío) were located in areas dominated by *Q. pyrenaica*, the forest type with the largest cover in the region, whilst the other three sites (Calzada de Tera, La Lora and Arcones) were located in areas dominated by *Q. ilex*, *Q. faginea*, and *J. thurifera*, respectively (Fig. 1b, Supplementary file S1).

Field sampling and estimation of plot-level carbon stocks

In each of the sites, in the areas occupied by abandoned agricultural lands, we located six 0.0625-ha plots (30 plots in total; Supplementary file S1), of identical slope and aspect according to the 1:50,000 National Digital Terrain Model obtained at Centro Nacional de Información Geográfica, and of identical land-use history according to local expert knowledge. We considered an area of 0.0625 ha because that was approximately the mean size of the abandoned agricultural fields in all sites, allowing for plots with uniform land use history. We conducted the field sampling between autumn 2018 and spring 2019. In each plot, we mapped and identified to species all tree and shrub individuals ≥ 0.25- and 0.50-m height, respectively. For trees ≥ 1.3-m height, we recorded the diameter at breast height (DBH; cm) by using a large calliper, and the height (H; m) by using a vertex hypsometer (Häglof, Sweden). In shorter (i.e. sapling) trees and shrubs, we measured diameter at root collar (DRC; cm) using callipers, and height (H; m) and the two main canopy diameters (CD; cm) using a measuring tape.

To estimate plot-level C stocks, we first calculated the above-ground biomass (AGB; Mg ha^{-1}) per individual through allometric equations for both tree and shrub species (Supplementary file S2). For the dominant tree species in the study sites (i.e. *J. thurifera*, *Q. faginea*, *Q. ilex*, and *Q. pyrenaica*) as well as for *Pinus pinaster* and *P. sylvestris*, we also calculated the below-ground biomass (BGB; Mg ha^{-1}) per individual. Most of these equations were species-specific and developed for nearby regions. Second, we summed up the individual-level biomass values calculated, to obtain plot-level estimates of AGB and BGB (Mg ha^{-1}). Finally, these biomass values were transformed into plot level AGC and BGC stocks (Mg C ha^{-1}) using species-specific conversion factors (e.g. Montero et al. 2005), where they existed, and when not, by using the default value of 0.5 (Penman et al. 2003).

Radar data processing

We used scenes from the L-band (23.6-cm wavelength) *Advanced Land Observing Satellite—Phased Array L-band Synthetic Aperture Radar* (ALOS-PALSAR) sensor, because they are particularly well suited for estimating the AGC stocks in forests with low biomass (i.e. < 75 Mg C ha^{-1}; McNicol et al. 2018), strong spatial heterogeneity (Mitchard et al. 2009), and vertical stratification (i.e. showing woody individuals of different ages or regrowth phases; Joshi et al. 2017), such as those existing in areas subjected to spontaneous revegetation after agricultural land abandonment in Mediterranean environments (Alivernini et al. 2016). We acquired the scenes covering the entire study area for the year 2018 at the *Earth Observation Research Center* (EORC). These scenes were in the Fine Beam Dual (FBD) mode, which provide HH and HV data with an incidence angle of 30–40°, and a pixel size of 25 m × 25 m (Shimada et al. 2014), and were mainly collected in summer (Supplementary file S3). They were all geometrically and slope corrected, and radiometrically calibrated. We first mosaicked all scenes into one and converted the SAR backscatter from digital number to decibel (i.e. $sigma^0$, db) values using the revised calibration coefficients of Shimada et al. (2014). Then, we reduced the speckle and noise through an Enhanced Lee filter with a 5 × 5 window (McNicol et al. 2018). Third, we masked the resulting scene using the digitised area of the recovering lands, which was obtained by superimposing the 1977–1980 orthophotos and the areas occupied by the four forest types according to the *Spanish Forest Map* (e.g. Laurin et al. 2018). Finally, we calculated the mean $sigma^0$ (db) SAR backscatter for HH and HV polarisations for those pixels occupying the area of each of the 30 study plots.

Regressions and development of carbon maps

We regressed plot-level values of SAR backscatter against total AGC density. As we had a relatively low number of plots (i.e. 30), we expected that these regressions could be fitted to the linear model (E. Mitchard, pers. communication); however, we also assessed their fit to six different non-linear asymptotic models usually considered in these types of studies (Supplementary file S4). Amongst all regression models, we selected the one (i) with the lowest number of terms; (ii) producing the lowest *Akaike Information Criterion* (AIC), *Residual Mean Squares Error* (RMSE), and *Residual Standard Error* (RSE) values; and (iii) explaining the highest proportion of variance (%) and/or showing the highest coefficient of determination (R^2) (Mitchard et al. 2009). In order to produce BGC maps, we additionally studied the relationships between AGC and BGC. For the relationships between SAR backscatter and AGC, we also performed an uncertainty analysis to assess the accuracy of the AGC estimates by obtaining the *Residual Mean Squared Errors* (RMSE) of the linear regressions between the values of AGC predicted by the models, and the observed plot-level AGC values (Mitchard et al. 2012). We used this analysis as second criteria to choose the best model (i.e. selecting the model producing the highest accuracy in the AGC estimates for all range of observed AGC values). Through the analysis of these relationships, we defined the range of values of AGC at which the finally chosen SAR backscatter ~ AGC model predicted AGC with the least uncertainty (Mitchard et al. 2011). We followed a similar approach to assess the uncertainty on the BGC estimates based on the AGC ~ BGC regression models.

To develop the AGC maps, we first rearranged the finally selected SAR backscatter ~ AGC model to AGC ~ backscatter

one. We proceed in that way because the SAR backscatter is a response to the structural elements of the vegetation and the soil once the radar beam interacts with them, and therefore, it is subjected to a much larger variability than plot-level AGC density, which is directly estimated from field measurements. For this reason, it is better to perform model selection keeping AGC density as the independent variable, and once selected the best fitting model, rearrange it (Woodhouse 2006). We developed the AGC maps by using the rearranged AGC ~ backscatter regression model to convert pixel-level db values on the masked ALOS-PALSAR scenes to pixel-level AGC density (Mg C ha^{-1}) values. We also applied the finally selected AGC ~ BGC regression model to the same area to map BGC density (Mg C ha^{-1}). To obtain total AGC and BGC stocks (Tg), we multiplied pixel-level AGC and BGC densities by 0.0625 ha (i.e. the pixel size; 25 m × 25 m), and divided by 10^{-6} (i.e. the equivalence between Tg and Mg). Finally, we summed up all pixels within the areas affected by agricultural land abandonment. We got the AGC and BGC stocks rate of change (Tg C $year^{-1}$) by dividing AGC and BGC stocks by 40 years (the study period of 1977–2017).

We performed the mosaicking and cropping processes of ALOS-PALSAR scenes, as well as the propagation of the regression models, in QGIS v.3.10 (QGIS Development Team 2019), and the speckle and noise reduction processes in ESA-SNAP v.4.0.0 (ESA Sentinel Application Platform 2020) and ENVI 4.6 (ITT, Boulder, USA). All regression analyses were carried out with the BIOMASS (Réjou-Méchain et al. 2017), knitr (Xie 2022) and nlstools (Baty et al. 2015) R packages.

Results

Area affected by forest expansion in abandoned agricultural lands

All over the study region, 145,193 ha of the current forests dominated by *J. thurifera*, *Quercus faginea*, *Q. ilex*, and *Q. pyrenaica* corresponded to areas subjected to spontaneous revegetation in abandoned agricultural lands (Fig. 1b, Table 1), which represented 1.54% of the total area of *Castilla y León* and 12.12% of the total area occupied by these forests according to the *Spanish Forest Map* (~ 1.2 million of ha). With regard to the different forest types, 13.39% of the forests currently dominated by *Q. ilex* (i.e. 62,627 ha) and 9.23% of those dominated by *Q. pyrenaica* (i.e. 61,870 ha) were originated after agricultural land abandonment.

Relationships between Synthetic Aperture Radar backscatter and above-ground carbon

The results of the linear regressions between mean $sigma^0$ (db) SAR backscatter values and AGC density values for all plots of the study area gave a larger coefficient of determination for HV ($R^2 = 0.26$, $P < 0.05$) than for HH ($R^2 = 0.18$, $P < 0.05$) polarisations. Therefore, we just considered HV polarisations to assess the SAR backscatter ~ AGC relationships and for the uncertainty analysis. Although the two-parameter model of Mitchard et al. (2009) gave the best fit (Supplementary file S5), the linear regression between HV-predicted and observed AGC density values yielded larger overall root mean square error (RMSE) values when considering this model (57.63 Mg C ha^{-1}; Supplementary file S6b) than the linear one (23.44 Mg C ha^{-1}; Supplementary file S7b). Moreover, the errors in the HV-predicted AGC according to two-parameter model of Mitchard et al. (2009) were very large for the entire range of AGC values observed (Supplementary file S6b), whereas, according to the linear model, they were just large for plots with small values of AGC, i.e. < 1 Mg C ha^{-1} (Supplementary file S7b,c). Consequently, to estimate AGC density from mean HV $sigma^0$ backscatter values, we finally choose the linear model. From this linear model, we excluded five outlier plots from analysis (113, 123, 323, 413, and 513), because they showed extraordinarily large mean HV $sigma^0$ backscatter values with regard to the low AGC density they accumulated (Supplementary file S1). For this finally chosen linear model ($R^2 = 0.37$, $P < 0.05$; Fig. 2a), we obtained a RMSE of 18.98 Mg C ha^{-1} (Fig. 2c) which decreased up to 15.35 Mg C ha^{-1} if only values of observed AGC > 1 Mg C ha^{-1} were considered, and to 14.96 Mg C ha^{-1} using just plots with

Table 1 Main characteristics of the four forests types differentiated within the study region according to dominant tree species based on the *Spanish Forest Map*; total area, area currently occupied by recovering lands, proportion of the total area currently occupied by recovering lands, mean above- and below-ground carbon (AGC and BGC) densities (Mg C ha^{-1}) and stocks (Tg)

Forest type	Area (ha)	Area of recovering lands (ha)	Proportion occupied by recovering lands (%)	AGC density (Mg C ha^{-1})	AGC stock (Tg C)	BGC density (Mg C ha^{-1})	BGC stock (Tg C)
Juniperus thurifera	80.724	10.910	7.26	22.52	0.29	7.56	0.1
Quercus faginea	79.146	9.787	3.62	12.84	0.19	4.53	0.07
Quercus ilex	424.536	62.627	13.39	13.76	3.36	5.14	0.39
Quercus pyrenaica	612.727	61.870	9.23	23.03	2.43	9.03	3.17
Total	1.197.133	145.193	12.13	18.04	6.27	6.56	3.73

observed AGC > 0.7 Mg C ha^{-1}. However, when considering plots with observed AGC > 0.5 Mg C ha^{-1}, RMSE increased up to 17.72 Mg C ha^{-1}. Therefore, the finally selected linear model was of the form:

$$HV = -16.7493 + (0.0873 \times AGC) \quad (1)$$

where HV is the mean HV *sigma*^{0} (db) SAR backscatter, and AGC is the C content in Mg C ha^{-1}, per plot. In order to develop the HV-predicted AGC maps, this equation was rearranged to:

$$AGC = (HV + 16.7493)/0.0873 \quad (2)$$

The large bias observed for AGC values < 0.7 Mg C ha^{-1} (Fig. 2c) suggested that we should not use this model to estimate ACG below this point. Moreover, in order to avoid the estimation of the AGC stored in the large remnant trees located in field edges and nearby areas, we used the model to estimate AGC density just up to the largest plot-level value observed (i.e. 60 Mg C ha^{-1}; Supplementary file S1). When using the model to create AGC density maps based on mean HV *sigma*^{0} (db) backscatter values, we considered AGC density classes similar in size to the RMSE values found, from the minimum value of AGC giving an acceptable RMSE and up to the largest value of AGC density observed in the plots: < 0.7, 0–15, 15–30, 30–45, 45–60, and > 60 Mg C ha^{-1}.

Relationships between above- and below-ground carbon

The linear regression between plot-level AGC and BGC density values for all plots gave a very large coefficient of determination ($R^2 = 0.82$, $P < 0.001$; Supplementary file S8). According to the uncertainty analysis for this relationship, however, the linear regression between AGC-predicted and BGC-observed values yielded relatively small RMSE values with the exception of plot 121, which was considered an

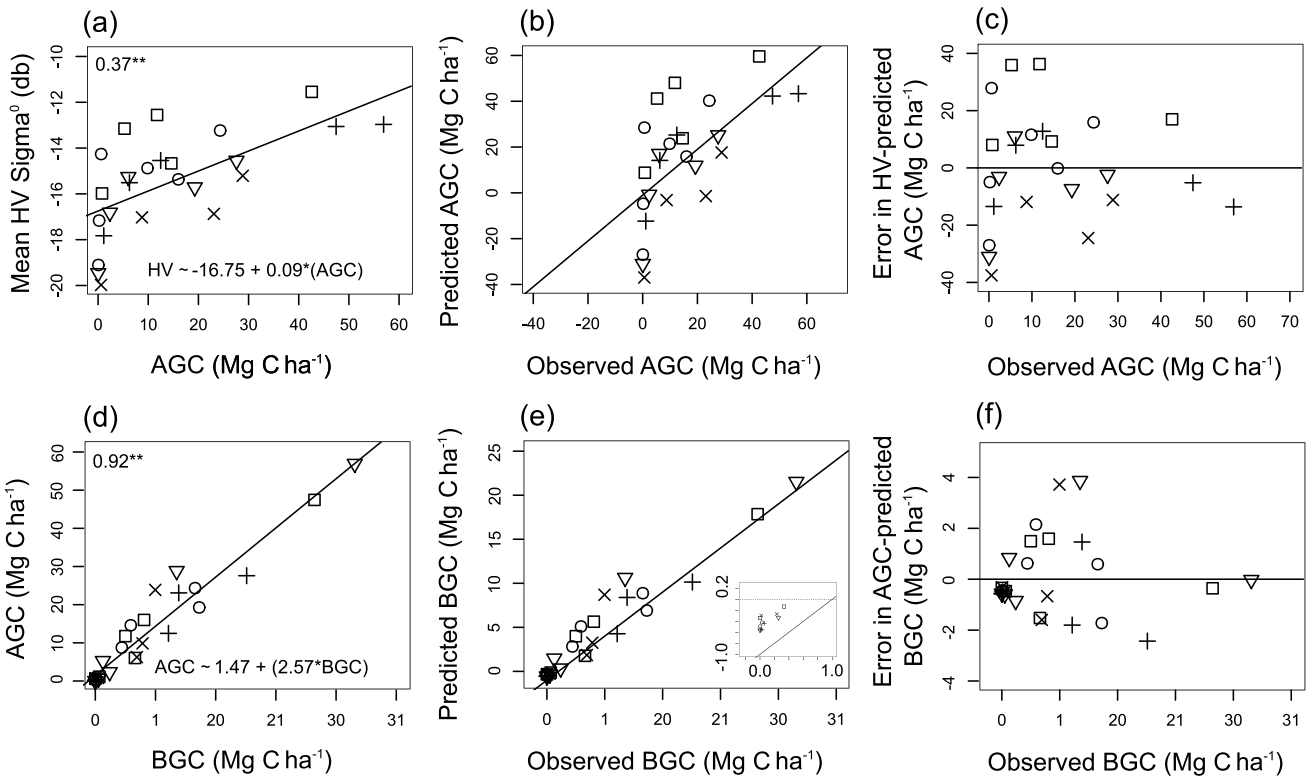

Fig. 2 Prediction of AGC from the mean HV *sigma*^{0} (db) SAR backscatter and its uncertainty analysis: (**a**) linear regression between the mean HV *sigma*^{0} SAR backscatter values and plot-level above-ground carbon (AGC; Mg C ha^{-1}); (**b**) plot-level AGC predicted from mean HV *sigma*^{0} (db) SAR backscatter according to the linear model considering 25 plots, plotted against observed (i.e. estimated through direct field measurements) AGC, with an $x = y$ line shown; (**c**) error in HV-predicted AGC plotted against observed AGC for the entire range of AGC values found (i.e. 0–60 Mg C ha^{-1}). Prediction of BGC from AGC and its uncertainty analysis: (**d**) linear regression between plot-level above- and below-ground carbon (AGC and BGC, respectively; Mg C ha^{-1}); (**e**) plot-level BGC predicted from AGC according to the linear model considering 29 plots, plotted against observed BGC, with an $x = y$ line shown, and a detail for predicted BCG < 0,25 Mg C ha^{-1} plotted against observed BGC < 1 Mg C ha^{-1}, included as an inset; (**f**) error in AGC-predicted BGC plotted against observed BGC for the entire range of BGC values found (i.e. 0–25 Mg C ha^{-1}). All other specifications are as in Fig. 1

outlier and subsequently, it was removed. Once removed this plot, the fitting of the model improved ($R^2 = 0.92$, $P < 0.001$; Fig. 2d), and the accuracy of the BGC predictions was similar for the entire ranges of BGC values observed (Fig. 2e). Therefore, the finally selected linear model was of the form:

$$AGC = 1.4734 + (2.5758 \times BGC) \quad (3)$$

In order to develop the AGC-predicted BGC maps, this equation was rearranged to;

$$BGC = (AGC - 1.4734)/2.5758 \quad (4)$$

The overall root mean square error (RMSE) for this model was 2.41 Mg C ha^{-1}, which decreased to 1.76 Mg C ha^{-1} if only values of BGC > 0.5 Mg C ha^{-1} were considered (Fig. 2f). Therefore, we used this model to create BGC density maps from BGC > 0.5 Mg C ha^{-1} onwards. We considered the same classes for BGC as for AGC to enhance a better comparison between both maps.

Carbon maps

We produced AGC and BGC density (Mg C ha^{-1}) maps for all the area occupied by recovering lands (Fig. 1b), but here, in order to save space, we just show the AGC density maps restricted to areas immediately around the five study sites (Fig. 3a–e). From our AGC map, and considering just pixels with AGC density values between 0.7 and 60 Mg C ha^{-1}, we estimated that, between 1977 and 2017, AGC density in areas subjected to spontaneous revegetation of abandoned agricultural lands recovered a mean of 18.04 Mg C ha^{-1}. However, we detected large variations between forest types; the largest mean AGC density values were in the areas dominated by *Q. pyrenaica* and *J. thurifera* (23.03 and 22.52 Mg C ha^{-1}, respectively), and the smallest, in the areas dominated by *Q. ilex* and *Q. faginea* (i.e. 13.76 and 12.83 Mg C ha^{-1}, respectively). With regard to the different AGC density classes considered, abandoned lands with mean AGC density values between 0.7 and 15 Mg C ha^{-1} occupied the largest area within the study region (Fig. 3f), whereas those with values between 15 and 30 Mg C ha^{-1} accounted for the largest AGC stocks (Fig. 3g). In all recovering lands of the study region, over the last 40 years (Fig. 1b), we estimated a total AGC stock of 6.27 Tg C, 92.34% of which corresponded to forests dominated by *Q. ilex* (3.36 Tg C) and *Q. pyrenaica* (2.43 Tg C). The rate of C sequestration of the AGC pool, over the period 1977–2017, was 0.16 Tg C·year^{-1}.

Below-ground C recovered a mean of 6.56 Mg C ha^{-1}, reaching larger values in forests dominated by *Q. pyrenaica* (9.03 Mg C ha^{-1}) and *J. thurifera* (7.55 Mg C ha^{-1}; Table 1). A total of 3.73 Tg C was stored in BGC in recovering lands across the study region, from 1977 to 2017. The largest part of this stock (3.17 Tg; 83.4%) corresponded to forests dominated by *Q. pyrenaica* (Table 1). The rate of BGC stock change over the period 1977–2017 was 0.09 Tg C·year^{-1}.

Discussion

Relationships between Synthetic Aperture Radar backscatter and above-ground carbon

Overall, our findings indicate that, as long as the vegetation was dominated by sufficiently large tree structures, AGC could be predicted using SAR data for large regions comprising different vegetation types, being HV polarizations more appropriate than HH to estimate AGC density. These results confirm those previously found for mature forests in boreal (Sandberg et al. 2011) and tropical (Mitchard et al. 2009, 2011, 2012; McNicol et al. 2018) environments. It is important to point out that AGC density estimations from mean HV $sigma^0$ SAR backscatter values clearly improved (i.e. the model showed smaller RMSE values) when excluding certain recently abandoned plots (i.e. 113, 123, 323, 413, and 513). This might be explained by the instability of SAR backscatter from small-sized (< 0.1 ha) plots with heterogeneous vegetation structure (Sandberg et al. 2011). In fact, these five plots, mainly occupied by small shrubs and juvenile trees, were surrounded by mature forests and earlier-abandoned fields in which larger trees appeared (E. Velázquez, pers. observation). This small-scale spatial heterogeneity could be responsible of the distortions detected in the relationships between mean HV $sigma^0$ SAR backscatter and AGC density at small (< 0.7 Mg C ha^{-1}) AGC values, as the large trees present in neighbouring areas, give larger values of backscatter than the shrubs and juvenile trees present inside the plots (Laurin et al. 2018).

Area affected by agricultural land abandonment

The area occupied by abandoned agricultural lands comprised 1.54% of the total area of the study region, a larger proportion than those reported in Western Ukraine (Kuemmerle et al. 2011; 1.12%) and former USSR (Vuichard et al. 2008; 0.76%), which highlights the outstanding importance of the process of agricultural land abandonment at regional scale in Mediterranean continental environments (Lasanta et al. 2021). Moreover, abandoned agricultural lands were mostly located near the mountain ranges surrounding the study area, even in sites close to large population centres and main transportation routes (Fig. 1b). This suggests that the causes of abandonment were related to the strong physical constraints to

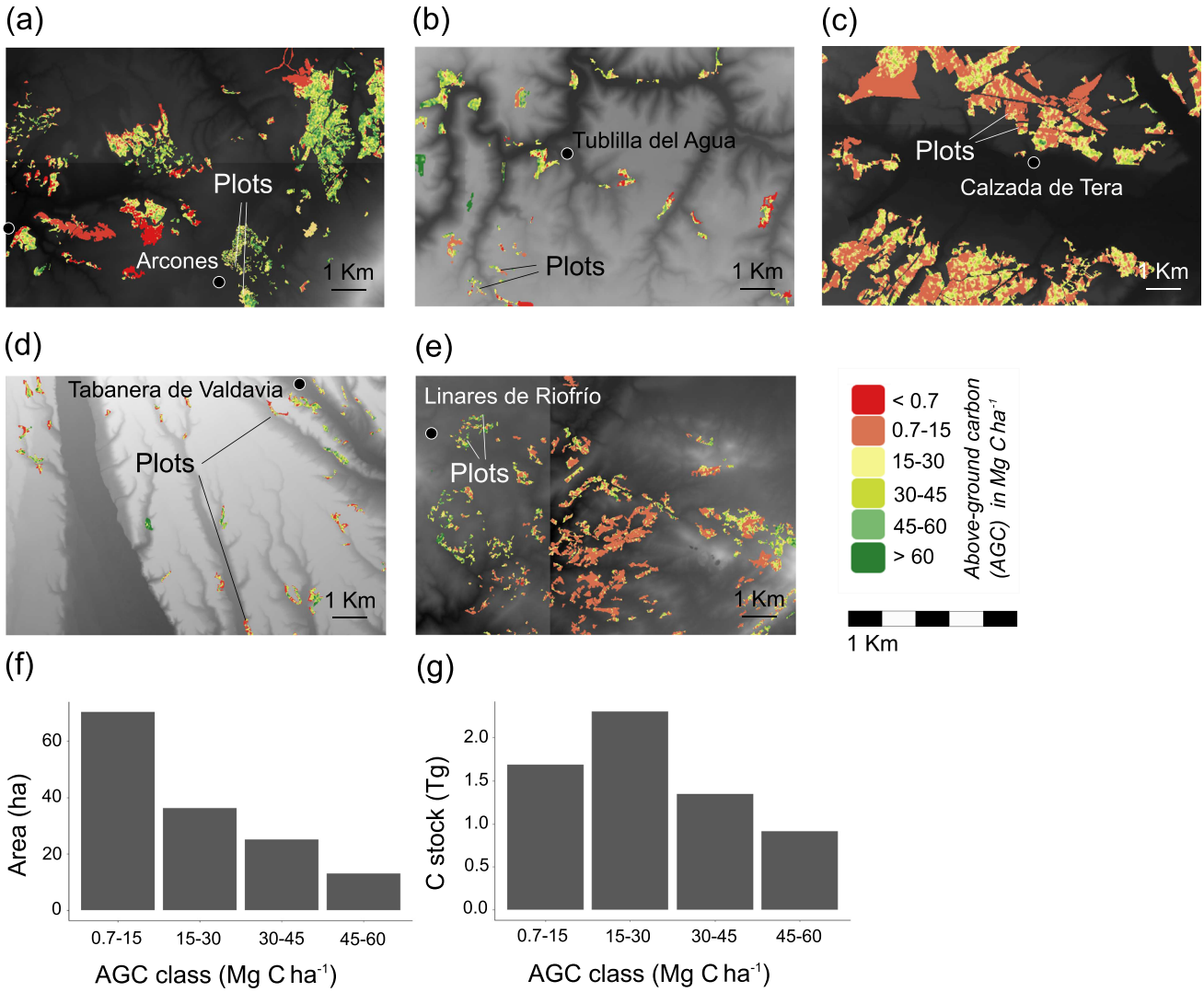

Fig. 3 Maps of above-ground carbon (AGC; Mg C ha^{-1}) density estimated through the linear regression model between mean HV $sigma^0$ SAR backscatter and AGC values, in the new recovering lands of (**a**) Arcones, (**b**) La Lora, and (**c**) Calzada de Tera, where they are dominated by *Juniperus thurifera*, *Quercus faginea*, and *Q. ilex*, respectively, and in (**d**) La Valdavia and (**e**) Linares de Riofrío, where they are dominated by *Q. pyrenaica*. These maps are represented over a Digital Terrain Model and considering six AGC density classes which include the four considered in the study to compute the total C stocks and rates: 0.7–15, 15–30, 30–45, and 45–60 Mg C ha^{-1}. For each of these classes, (**f**) the total area occupied (ha) and (**g**) the above-ground carbon (AGC) stocks (Tg) are also indicated

cultivation (i.e. low fertility soils, stoniness, relatively steep slopes) found in these areas (C. del Peso-Taranco, pers. observation). We detected many areas in which forest expansion in abandoned agricultural lands had apparently occurred (i.e. areas that were occupied by crop or pasture lands according to the ortho-corrected images of 1977–1980, and by woody vegetation according to those of 2015–2017), but that were not identified as *forests* by the *Spanish Forest Map*. However, as they could not be associated to any of the four forests types selected, we did not finally consider them. Moreover, as we were constrained by budget and time limitations, we just focus on the four main forest types all over the study region, but not in others such as those dominated by the prickly juniper (i.e. *J. oxycedrus*) which, although covering a smaller total area, could have also partially developed in abandoned agricultural lands (del Peso-Taranco and Bravo 2006). All this evidence indicates that the area affected by agricultural land abandonment could be even larger than estimated in this study. Here, it is important to mention that, although forests dominated by *Pinus pinaster* and *P. sylvestris* also occupied a large area all over the study region, they were not considered because (i) the extensive use of these species in plantations between 1960 and 1990 made very difficult the identification of naturally regenerated areas when comparing the aerial photographs of 1977–1980 and 2017–2019, and (ii) in our field surveys, we did not observed pine forests developed from spontaneous colonisation.

Carbon densities, stocks, and sequestration rates

The mean value of AGC density found (18.04 Mg C ha^{-1}) was low considering that the recovering lands detected had developed over 40 years. For instance, Alivernini et al. (2016) found a mean AGC density of 21.1 Mg C ha^{-1} in forests developed after agricultural abandonment over the period 1990–2012, in a temperate area of Central Italy. In our study, located in a Mediterranean continental environment, the minimum values of AGC density detected were similar to those found by Calvão and Palmeirim (2004; 0.36 Mg C ha^{-1}) in Portuguese shrublands developed in abandoned agricultural lands. We found, however, a relatively large maximum AGC density (i.e. 60 Mg C ha^{-1}). This value is similar to those reported by Vayreda et al. (2011; 45 Mg C ha^{-1}) for Spanish forests and Pan et al. (2011; 75 Mg C ha^{-1}) for world temperate forests, but lower to those reported by Houghton et al. (2009; 80–135 Mg C ha^{-1}) and Laurin et al. (2018; 182.5 Mg C ha^{-1}) for world temperate forests, also. The relatively large maximum AGC densities that we have found might be explained by the high wood C content of Mediterranean (45.7–60.7%) comparing to temperate (43.4–55.6%) tree species (Thomas and Martin 2012). In fact, 54% of the estimated total AGC stock (i.e. 3.36 of 6.27 Tg C) corresponded to forests dominated by *Q. ilex*, which stores a large C content in its biomass and it is usually used as firewood (Montero et al. 2005).

The total AGC stock detected (6.27 Tg C) was modest considering the large study area of *Castilla y León* (9.4 million ha), equivalent to 0.6 Tg C · million ha^{-1}. To compare, according to the third *National Forest Inventory* (2006), the total AGC forest stocks in *Castilla y León* and Spain (50.59 million ha) were estimated as 67.8 (Gil et al. 2011) and 627 (Vayreda et al. 2011) Tg C, equivalent to 7.21 and 12.39 Tg C · million ha^{-1}, respectively. In a similar study performed in European Russia, Ukraine, and Belarus (30.8 million ha), Schierhorn et al. (2013) found 470 Tg of AGC (equivalent to 15.25 Tg C · million ha^{-1}) accumulated following agricultural land abandonment over the period 1991–2001. The modest AGC stock found can be explained by the fact that pixels accounting for low (i.e. 0.7–15 Mg C ha^{-1}) AGC density occupied the largest area all over the study region (Fig. 3f). Proportionally, the BGC stock (i.e. 3.73 Tg C) was relatively large, contributing 37.3% of the total C stock (i.e. 10 Tg C), which contrasts with the 21.9% (54 Gt C for a total number of 247 Gt C) found by Saatchi et al. (2011) for tropical ecosystems. This is not surprising since investment in deep root biomass is a main feature of deciduous or semi-deciduous trees in Mediterranean continental environments, allowing them to maintain high evapotranspiration rates during summer months, when water availability is limited (Moreno et al. 2011). In fact, forests dominated by *Q. pyrenaica* (a marcescent oak) made up 85% of the total BGC stock (i.e. 3.17 of 3.73 Tg C; Table 1). Additionally, the largest AGC and BGC stocks occurred in the *Q. pyrenaica* forests of the westernmost sections of the Cantabrian and Central Ranges (Fig. 1b); the zones comprising the highest mean annual rainfall values over the study area (i.e. ≥ 1000 mm · $year^{-1}$; Ninyerola et al. 2005). These results resemble those of Schierhorn et al. (2013), which detected the largest AGC stocks in the wettest parts of European Russia, Ukraine, and Belarus, and suggest that in geographical regions where mean annual rainfall is highly variable, such as Central-North Iberian Peninsula, it may be a major determinant of forest expansion in abandoned agricultural lands.

It is also important to note that, considering both, AGC and BGC, we detected a mean annual C sink of 0.25 Tg C·$year^{-1}$. Therefore, C sequestration in the 145.2 kha of recovering lands detected, just compensated for 1.22% of total CO_2 emissions (28.19 Tg C·$year^{-1}$) in *Castilla y León*, between 1990 and 2018 (MITECO 2022). The potential of forest expansion in abandoned agricultural lands to offset regional CO_2 emissions seems therefore limited. However, most of the study area was occupied by abandoned agricultural lands with mean AGC density values between 0.7 and 15 Mg C ha^{-1} (Fig. 3f), and in a parallel research, dendroecological analysis has shown a 15–20-year lag between land abandonment and tree colonisation. These facts suggest that in many of these lands spontaneous revegetation has still not reached its peak.

Conclusions and further implications

To our knowledge, this is the first assessment of C accumulation as a consequence of forest expansion in abandoned agricultural lands at regional scale, over the last few decades, in Mediterranean continental environments. Our results indicate that in these types of environments, spontaneous revegetation after agricultural abandonment is a highly relevant LULUC process, occurring over large areas; however, the mean C densities and total C stocks developed as a consequence of this process are relatively low, with an extraordinarily high contribution of the below-ground biomass to the total C stock, and its C sink strength is apparently modest. These findings should be considered in such a context in which the ability of these recovering lands to accumulate more C can be negatively affected by the decrease in precipitation that has been predicted by climatic models for the Mediterranean basin over forthcoming decades (Kovats et al. 2014). A similar negative effect can be expected if droughts, heat waves, and fires (Sitch et al. 2015), as well as outbreaks of pests and pathogens (Casazza et al. 2021), become more severe and/or frequent as a consequence of the increase in mean annual temperature.

However, the potential for atmospheric CO_2 sequestration in recovering lands in this area of Central-North Spain should not be underestimated. First, because the area affected by agricultural land abandonment could be larger than estimated in this study, and second, because in many of the recovering

lands detected, C accumulation may have not reached its peak. Moreover, in these recovering lands, live forest C accumulation might be enhanced by means of active measures of forest management such as tree pruning and thinning, which improve individual's growth (Aldea et al. 2017) and forest resilience after dry periods (Sohn et al. 2016). Our results are also important when considering that, as forest expansion in abandoned agricultural lands has also occurred in many other inland regions of the Northern Mediterranean basin (Beilin et al. 2014), countries such as Spain, Portugal, Italy, and Greece could redefine their national-scale GHG emission reduction commitments by including the C sinks generated by this process as afforestation activities (Alivernini et al. 2016). Summarising, our findings highlight the importance of forest expansion in abandoned agricultural lands as a major land use change in Mediterranean continental environments, where this process has done their part on increasing atmospheric CO_2 sequestration, and therefore, in mitigating the effects of climate change. How to preserve the C sink generated avoiding its release as a consequence of the negative effects of climate change, and how to increase it though active measures of forest management remain as remarkable targets for the upcoming decades.

Supplementary Information The online version contains supplementary material available at https://doi.org/10.1007/s10113-022-01978-0.

Acknowledgements This study was initially based on inspiring ideas from A. Escudero and J. Vayreda. We are also grateful to C. del Peso for his comments on the land-use history of the study area, and to I. Molina, C. Villar, C. Allue, M.A. Llamas, and J.M. Martínez from the *Regional Environmental Service* of the Government of the Autonomous Community of *Castilla y León* to give us the permissions to work in public lands all over the study sites. We also acknowledge the predisposition of M. Herrero, T. and P. Zarza, Mª.I. Martín, and I. Alonso to allow us to work in their lands in Linares de Riofrío. The fieldwork could be successfully finished thanks to the inestimable help provided by F. Ampudia, E. Cudjoe, H. Galvis, V. García, S. Gutiérrez, S. Horzov, A. Martín, A. Mihn, C. Ordóñez, and M. Suárez, amongst others. We are also grateful to R. Ruiz-Peinado for his tips on the use of species-specific allometric equations and to L. Lassaletta and E. Uhl for their comments on earlier versions of the manuscript.

Funding Open Access funding provided thanks to the CRUE-CSIC agreement with Springer Nature. This study has been funded by the European Commission through the project CASE-CO2 (H2020-MSCA-IF-2017, DLV; 799885).

References

Aggenbach CJS, Kooijman AM, Fujita Y, van der Hagen H, van Til M, et al. (2017) Does atmospheric nitrogen deposition lead to greater nitrogen and carbon accumulation in coastal sand dunes? Biol Conserv 212:416–422. https://doi.org/10.1016/j.biocon.2016.12.007

Aldea J, Bravo F, Bravo-Oviedo A, Ruiz-Peinado R, Rodríguez F, et al. (2017) Thinning enhances the species-specific radial increment response to drought in Mediterranean pine-oak stands. Agric For Meteorol 237:371–383. https://doi.org/10.1016/j.agrformet.2017.02.009

Alivernini A, Barbati A, Merlini P, Carbone F, Corona P (2016) New forests and Kyoto Protocol carbon accounting: a case study in central Italy. Agric Ecosyst Environ 218:58–65. https://doi.org/10.1016/j.agee.2015.11.006

Allende-Álvarez F, Guerra-Velásco JC, López-Estebánez N (1997) La dinámica reciente de los sabinares albares españoles. In: SECF (ed) III Congreso Forestal Español, Tomo I, Granada, pp 334–336

Barbier EB, Burgess JC, Grainger A (2009) The forest transition: towards a more comprehensive theoretical framework. Land Use Policy 27:98–107. https://doi.org/10.1016/j.landusepol.2009.02.001

Baty F, Ritz C, Charles S, Brutsche M, Flandrois JP, Delignette-Muller ML (2015) A toolbox for nonlinear regression in R: the package nlstools. J Stat Softw 66(5):1–21. https://doi.org/10.18637/jss.v066.i05

Beilin R, Lindborg R, Stenseke M, Pereira HM, Llausàs A, et al. (2014) Analysing how drivers of agricultural land abandonment affect biodiversity and cultural landscapes using case studies from Scandinavia, Iberia and Oceania. Land Use Policy 36:60–72. https://doi.org/10.1016/j.landusepol.2013.07.003

Calvão T, Palmeirim J (2004) Mapping Mediterranean scrub with satellite imagery: biomass estimation and spectral behaviour. Int J Remote Sens 25:3113–3126. https://doi.org/10.1080/01431160310001654978

Canadell J, Jackson RB, Ehleringer JR, Mooney HA, Sala OE, et al. (1996) Maximum rooting depth of vegetation types at the global scale. Oecologia 108:583–595. https://doi.org/10.1007/BF00329030

Casazza G, Malfatti F, Brunetti M, Simonetti V, Mathews AS (2021) Interactions between land use, pathogens, and climate change in the Monte Pisano, Italy 1850–2000. Landsc Ecol 36:601–616. https://doi.org/10.1007/s10980-020-01152-z

Chrysafis I, Mallinis G, Siachalou S, Patias P (2017) Assessing the relationships between growing stock volume and Sentinel-2 imagery in a Mediterranean forest ecosystem. Remote Sens Lett 8:508–517. https://doi.org/10.1080/2150704X.2017.1295479

Cramer VA, Hobbs RJ, Standish RJ (2008) What's new about old fields? Land abandonment and ecosystem recovery. Trends Ecol Evol 23:104–112. https://doi.org/10.1016/j.tree.2007.10.005

del Peso-Taranco C, Bravo F (2006) Los enebrales de *Juniperus oxycedrus* L. en el paisaje forestal del Valle del Alberche (Ávila), In: Ecología y Gestión Forestal Sostenible (ed) III Coloquio Internacional sobre Sabinares y Enebrales, Tomo I, Soria, pp 247–255

ESA Sentinel Application Platform (2020) SNAP-ESA Sentinel Application Platform v2.0.2. http://step.esa.int

Galidaki G, Zianis D, Gitas I, Radoglu K, Karathanassi V, et al. (2016) Vegetation biomass estimation with remote sensing: focus on forest and other wooded land over the Mediterranean ecosystem. Int J Remote Sens 7:1940–1966. https://doi.org/10.1080/01431161.2016.1266113

Gil MV, Blanco D, Carballo MT, Calvo LF (2011) Carbon stock estimates for forests in the Castilla y Leon region, Spain. A GIS based method for evaluating spatial distribution of residual biomass for bio-energy. Biomass Bioenerg 35:243–252. https://doi.org/10.1016/j.biombioe.2010.08.004

Gil-Sánchez L, Torre-Antón M (2007) Atlas Forestal de Castilla y León, Tomo I: Claves del pasado. Junta de Castilla y León, Valladolid

Goetz SJ, Baccini A, Laporte NT, Johns T, Walker W, et al. (2009) Mapping and monitoring carbon stocks with satellite observations: a

comparison of methods. Carbon Balance Manag 4:2. https://doi.org/10.1186/1750-0680-4-2

Houghton RA (2010) How well do we know the flux of CO_2 from land-use change? Tellus B Chem Phys Meteorol 62:337–351. https://doi.org/10.1111/j.1600-0889.2010.00473.x

Houghton RA, Hall F, Goetz SJ (2009) Importance of biomass in the global carbon cycle. J Geophys Res 114:1–13. https://doi.org/10.1029/2009JG000935

Joshi N, Mitchard ETA, Brolly M, Schumacher J, Fernández-Landa A, Johannsen VK, Marchamalo M, Fensholt R (2017) Understanding "saturation" of radar signals over forests. Sci Rep-UK. https://doi.org/10.1038/s41598-017-03469-3

Kovats R, Valentini R, Bouwer LM, Georgopoulou E, Jacob D, et al. (2014). Europe. In: Barros VR, Field CB, Dokken DJ, Mastrandrea MD, Mach KJ, Bilir TE, Chatterjee M, Ebi KL, Estrada YO, Genova RC, Girma B, Kissel ES, Levy AN, MacCracken S, Mastrandrea PR, White LL (eds) Climate change 2014: impacts, adaptation, and vulnerability. Part B: Regional Aspects. Contribution of Working Group II to the Fifth Assessment Report of the Intergovernmental Panel on Climate Change. Cambridge University Press, United Kingdom, pp 1267–1326

Kuemmerle T, Olofsson P, Chaskovskyy O, Baumann M, Ostapowicz K, et al. (2011) Post-soviet farmland abandonment, forest recovery, and carbon sequestration in western Ukraine. Glob Chang Biol 17:1335–1349. https://doi.org/10.1111/j.1365-2486.2010.02333.x

Lasanta T, Nadal-Romero E, Korchani M, Romero-Díaz A (2021) Una revisión sobre las tierras abandonadas en España: de los paisajes locales a las estrategias globales de gestión. Cuad Invest Geog 47. https://doi.org/10.18172/cig.4755

Laurin GV, Balling J, Corona P, Mattioli W, Papale D, et al. (2018) Aboveground biomass prediction by Sentinel-1 multitemporal data in Central Italy with integration of ALOS2 and Sentinel-2 data. J Appl Remote Sens 12:e016008. https://doi.org/10.1117/1.JRS.12.016008

Lu D (2006) The potential and challenge of remote sensing-based biomass estimation. Int J Remote Sens 27:1297–1328. https://doi.org/10.1080/01431160500486732

McNicol I, Ryan CM, Mitchard ETA (2018) Carbon losses from deforestation and widespread degradation offset by extensive growth in African woodlands. Nat Commun 9. https://doi.org/10.1038/s41467-018-05386-z

Mitchard ETA, Saatchi SS, Woodhouse IH, Nangendo G, Ribeiro NS, et al. (2009) Using satellite radar backscatter to predict above-ground woody biomass: a consistent relationship across four different African landscapes. Geophys Res Lett 23. https://doi.org/10.1029/2009GL040692

Mitchard ETA, Saatchi SS, Lewis SL, Feldpausch TR, Woodhouse IH, et al. (2011) Measuring biomass changes due to woody encroachment and deforestation/degradation in a forest-savanna boundary region of Central Africa using multi-temporal L-band radar backscatter. Remote Sens Environ 11:2861–2873. https://doi.org/10.1016/j.rse.2010.02.022

Mitchard ETA, Saatchi SS, White LJT, Abernethy KA, Jeffery KJ, et al. (2012) Mapping tropical forest biomass with radar and spaceborne LiDAR in Lopé National Park, Gabon: overcoming problems of high biomass and persistent cloud. Biogeosciences 9:179–191. https://doi.org/10.5194/bg-9-179-2012

MITECO (2022) Inventario Nacional de Gases de Efecto Invernadero. Comunicación a la Comisión Europea en Cumplimiento del Reglamento (UE) Nº 525/2013. Ministerio para la Transición Ecológica y el Reto Demográfico, Madrid

Montero G, Ruiz-Peinado R, Muñoz M (2005) Producción de biomasa y fijación de CO_2 por los bosques españoles. Monografías INIA: Serie Forestal nº 13. Instituto Nacional de Investigación Agraria, Madrid

Moreno G, Gallardo JF, Vicente MA (2011) How Mediterranean deciduous trees cope with long summer drought? The case of *Quercus pyrenaica* forests in Western Spain. In: Bredemeier M et al (eds) Forest Management and the Water Cycle: An Ecosystem-Based Approach, Ecological Studies 212. Springer-Verlag, Berlin, pp 189–201

Ninyerola M, Pons X, Roure JM (2005) Atlas Climático Digital de la Península Ibérica. Metodología y Aplicaciones en bioclimatología y geobotánica. Universitat Autónoma de Barcelona Web. https://opengis.grumets.cat/wms/iberia/espanol/ES_MODEL.HTM. Accessed 14 July 2021

Pan Y, Birdsey RA, Fang J, Houghton R, Kauppi PE, et al. (2011) A large and persistent carbon sink in the world's forests. Science 6045:988–993. https://doi.org/10.1126/science.1201609

Penman J, Gytarsky M, Hiraishi T, Krug T, Kruge D, et al. (2003) Good practice guidance for land use, land-use change and forestry. Intergovernmental Panel on Climate Change, Geneva

QGIS Development Team (2019) QGIS Geographic Information System. Open Source Geospatial Foundation Project. https://qgis.osgeo.org

Réjou-Méchain M, Tanguy A, Piponiot C, Chave J, Hérault B, Goslee S (2017) Biomass: an R package for estimating above-ground biomass and its uncertainty in tropical forests. Methods Ecol Evol 8(9):1163–1167. https://doi.org/10.1111/2041-210X.12753

Rhemtulla JM, Mladenoff DJ, Clayton MK (2009) Historical forest baselines reveal potential for continued carbon sequestration. Proc Natl Acad Sci USA 106:6082–6087. https://doi.org/10.1073/pnas.0810076106

Saatchi SS, Harris NL, Brown S, Lefsky M, Mitchard ETA, et al. (2011) Benchmark map of forest carbon stocks in tropical regions across three continents. Proc Natl Acad Sci USA 108:9899–9904. https://doi.org/10.1073/pnas.1019576108

Sandberg G, Ulander LMH, Fransson JES, Holmgren J, Le Toan T (2011) L- and P-band backscatter intensity for biomass retrieval in hemiboreal forest. Remote Sens Environ 11:2874–2886. https://doi.org/10.1016/j.rse.2010.03.018

Schierhorn F, Müller D, Beringer T, Prishchepov AV, Kuemmerle T, et al. (2013) Post-soviet cropland abandonment and carbon sequestration in European Russia, Ukraine and Belarus. Glob Biogeochem Cycl 27:1–11. https://doi.org/10.1002/2013GB004654

Shimada M, Itoh T, Motooka T, Watanabe M, Shiraishi T, et al. (2014) New global forest / non-forest maps from ALOS PALSAR data (2007–2010). Remote Sens Environ 155:13–31. https://doi.org/10.1016/j.rse.2014.04.014

Sitch S, Friedlingstein P, Gruber N, Jones SD, Murray-Tortarolo G, et al. (2015) Recent trends and drivers of regional sources and sinks of carbon dioxide. Biogeosciences 12:653–679. https://doi.org/10.1038/s41561-018-0204-7

Sohn JA, Saha S, Bauhus J (2016) Potential of forest thinning to mitigate drought stress: a meta-analysis. For Ecol Manag 380:261–273. https://doi.org/10.1016/j.foreco.2016.07.046

Thomas S, Martin A (2012) Carbon content of tree tissues: a synthesis. Forests 3:332–352. https://doi.org/10.3390/f3020332

Vayreda J, Gracia M, Canadell JG, Retana J (2011) Spatial patterns and predictors of forest carbon stocks in Western Mediterranean. Ecosystems 15:1258–1270. https://doi.org/10.1007/s10021-012-9582-7

Vuichard N, Ciais P, Belelli L, Smith P, Valentini R (2008) Carbon sequestration due to the abandonment of agriculture in the former USSR since 1990. Global Biogeochem Cycl 22:1–8. https://doi.org/10.1029/2008GB003212

Woodhouse I (2006) Introduction to microwave remote sensing. CRC Press, Boca Ratón. https://doi.org/10.1201/9781315272573

Xie Y (2022) knitr: a general-purpose package for dynamic report generation in R. R package version 1.4. https://yihui.org/knitr/